

## Three-dimensional Navier-Stokes simulations of the workings of scroll compressors

Alain PICALET , David GENEVOIS\*

Danfoss Commercial Compressors, 1600 Trevoux ; France  
[a.picavet@danfoss.com](mailto:a.picavet@danfoss.com) ; [d.genevois@danfoss.com](mailto:d.genevois@danfoss.com)

\* Corresponding Author

### ABSTRACT

This paper presents a detailed study of the scroll compressor compression process. Three-dimensional Navier-Stokes simulations are performed from the intake of the scroll wraps to the exit of the compressor, using moving meshes and a real gas equation for R410A. A new meshing technique has been used, which generates high quality structured grids for the scroll set, and gives a significant reduction on CPU time whilst maintaining accuracy.

Various operating points and rotational speeds are computed and the results are compared with detailed pressure measurements. Comparisons between computed and measured data show very good agreement, for the compressor nominal operating point as well as for higher and lower pressure ratios. The over or under-compression, which is typical of these operating conditions, is well represented. The total computed flow rates are also very close to the measured data, and for every simulated operating point. These results show that the flow leakage occurring during the compression process is correctly modelled, which is a very important point for performance prediction.

Overall, this study shows that significant progress has been made for the modelling of compression processes in positive displacement machines.

### 1. INTRODUCTION

Following numerous detailed studies undertaken by Danfoss on the internal compression process, CFD simulations were performed on machines of the SH scroll compressor family. The use of high quality structured hexahedral grids to mesh the mobile parts of the compressors, the technical capability of commercial CFD codes and the high performance of computers allows the efficient modelling of these internal fluid flows.

The computations are undertaken for a wide range of operating points, at high or low pressure ratios and for various rotational speeds. The post-processed CFD results are compared with experimental data for the compressor global performance and internal pressure measurements (Picavet and Giniès, 2014). The comparisons show that the CFD can accurately predict compressor performance. The precise analysis of suction and exhaust flows, overshoot, backflow and leakage gives an indication of the losses, their nature, where they occur and the resulting possibilities for improving performance.

### 2. NUMERICAL MODEL

The computational domain is shown in figure 1 and consists of a suction volume starting from the crankcase, the pockets defined by the scrolls and the high pressure zone, or upper shell, of the machine. The mobile parts are meshed using the software Twinmesh. We define a fixed and a mobile wrap and a number of steps per revolution. Twinmesh defines a geometry for each scroll angle to be simulated and generates a high quality structured hexahedral mesh based on each geometry (see figure 2). We choose to divide the revolution by 180. This ensures an angular step of 2° which is low enough to allow proper interpolation in the compression pockets between the meshes of two successive time steps. The cell density in the sealing zones avoids the use of any user function to limit the

value of the leakage. The distance between the scrolls is the same for each sealing point and constant during the whole revolution. This is the parameter which drives the internal leakage when the compressor runs hence it is crucial to tune it properly to accurately compute the mass flowrate.

Danfoss compressors are equipped with tip seals located at the top of the static and orbiting scroll spirals. The central part of each spiral interacts with the discharge port, hence there is no tip seal present in this zone, due to the risk of the seal being pulled out of its groove. The assumption we make to model the tip seals is a perfect contact between the wraps and the scroll base plates, except in the part previously described, where we mesh a narrow piece of fluid domain of tip gap thickness, embedded with the rotoric parts defined in Twinmesh.

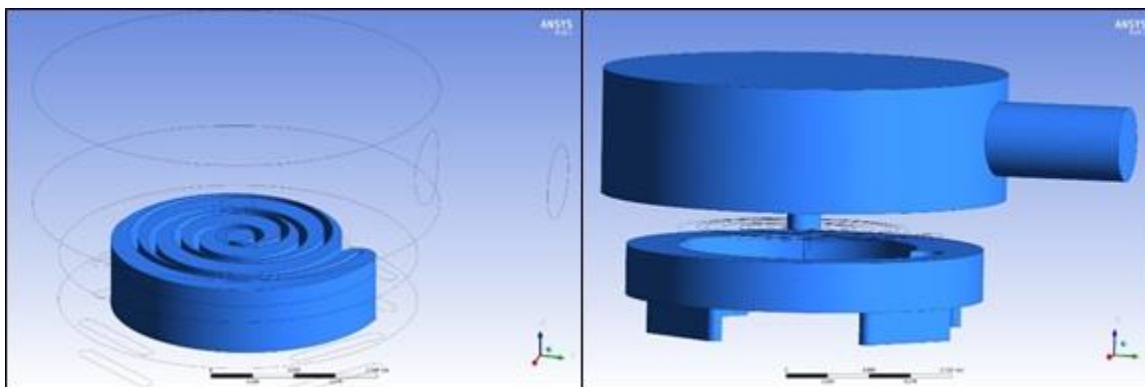


Figure 1 : computation domain – rotoric and statoric part

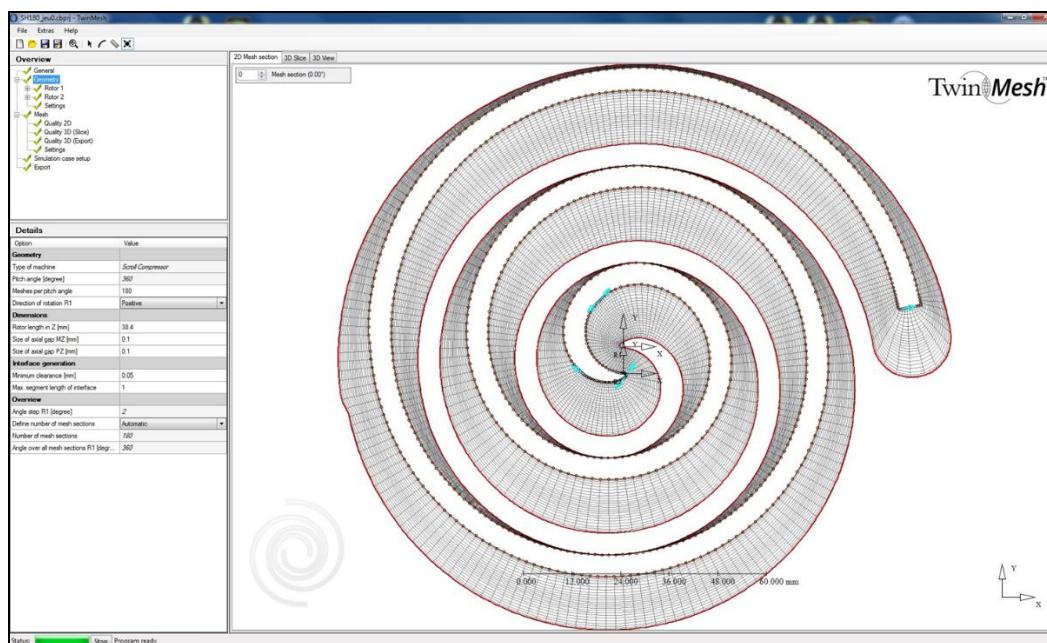


Figure 2 : moving mesh

The numerical model is based on the CFX software. Twinmesh generates a case file which has only to be completed in CFX by interfacing the stationary and rotating parts and setting up all the other features of the simulation (gas, velocity, monitoring data, etc.).

During the simulation, and for each angular step, CFX maps the computed flow field from the previous angular step onto the mesh at the current angular step. This method avoids the remeshing operations previously used with Fluent (Picavet and Angel, 2016) which, in addition to the quality of the grids, significantly reduces CPU time.

For all simulations:

- the flow is assumed to be unsteady, three-dimensional, compressible and turbulent with adiabatic walls.
- the gas is assumed to be a real gas, R410A, using the Peng-Robinson equation of state available in CFX to calculate fluid properties.
- turbulence is modeled using the shear-stress transport model.
- the boundary conditions used are “opening” (similar to pressure outlet) and wall.
- a second order scheme is used for equation discretisation.
- each operating point is run with 5 iterations per time-step during 3 revolutions, in order to reach a periodic regime. Then, 2 revolutions are completed with 10 iterations per time-step, to increase the accuracy of the computations.

The CFX simulations were run for various operating points: ARI and high and low pressure ratios. Various rotational speeds were also simulated: 2900 and 4400 rpm.

### 3. RESULTS AND DISCUSSION

#### 3.1 Mass flow rate

Figure 3 compares computed mass flow rates of a machine, at different operating points, with the values measured during a previous test campaign. As the boundary conditions of the simulations are of pressure type, the flowrate is a result of the computation and is highly dependent on the flow leakage. The good agreement between measured and predicted flow rates validates the choices made in terms of the leakage gap between scrolls at the sealing point locations and in terms of cell count in the gaps. It also shows that we can adequately predict the cooling or heating capacity of a scroll compressor using CFD. The ARI point corresponds to an evaporating temperature of 7.2 °C and the condensing one to 54.4 °C.

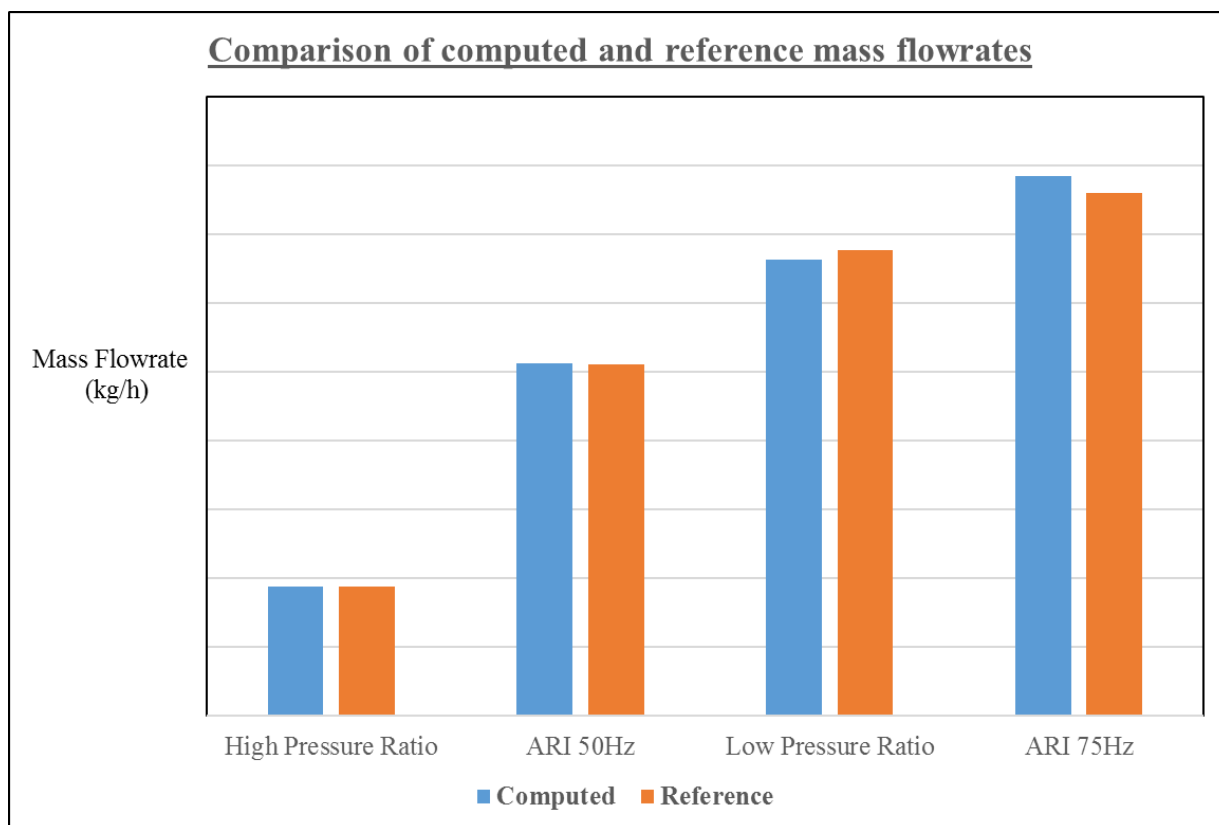
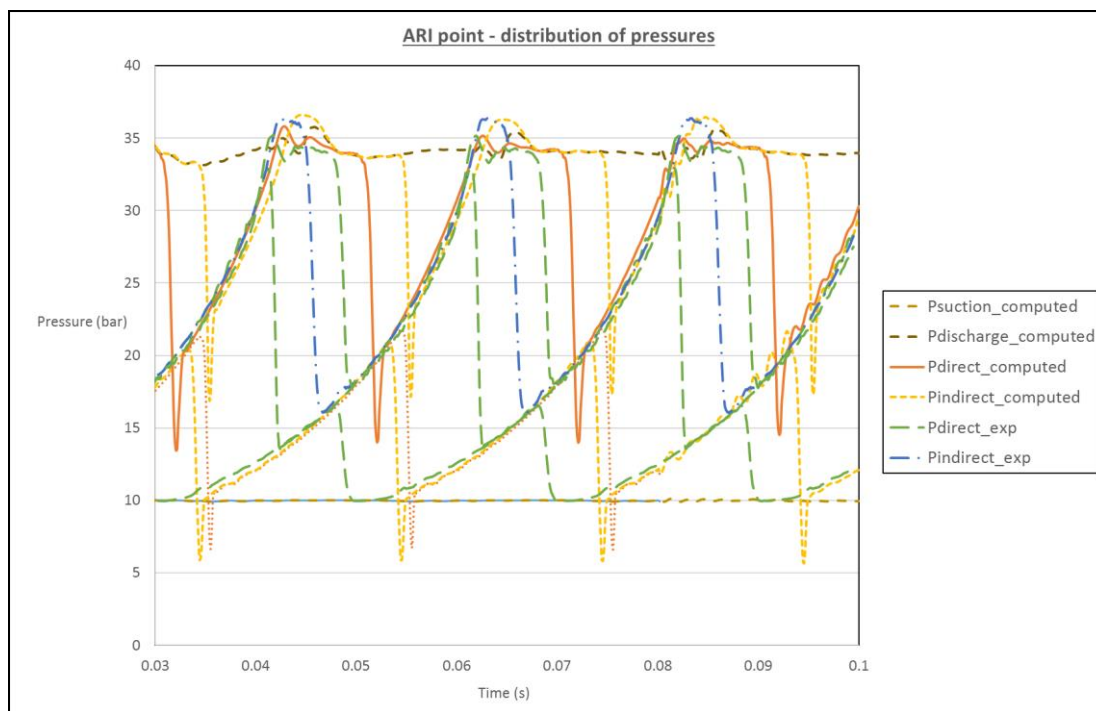


**Figure 3** : comparison between measured and computed mass flowrates

### 3.2 Analysis of pressure curves

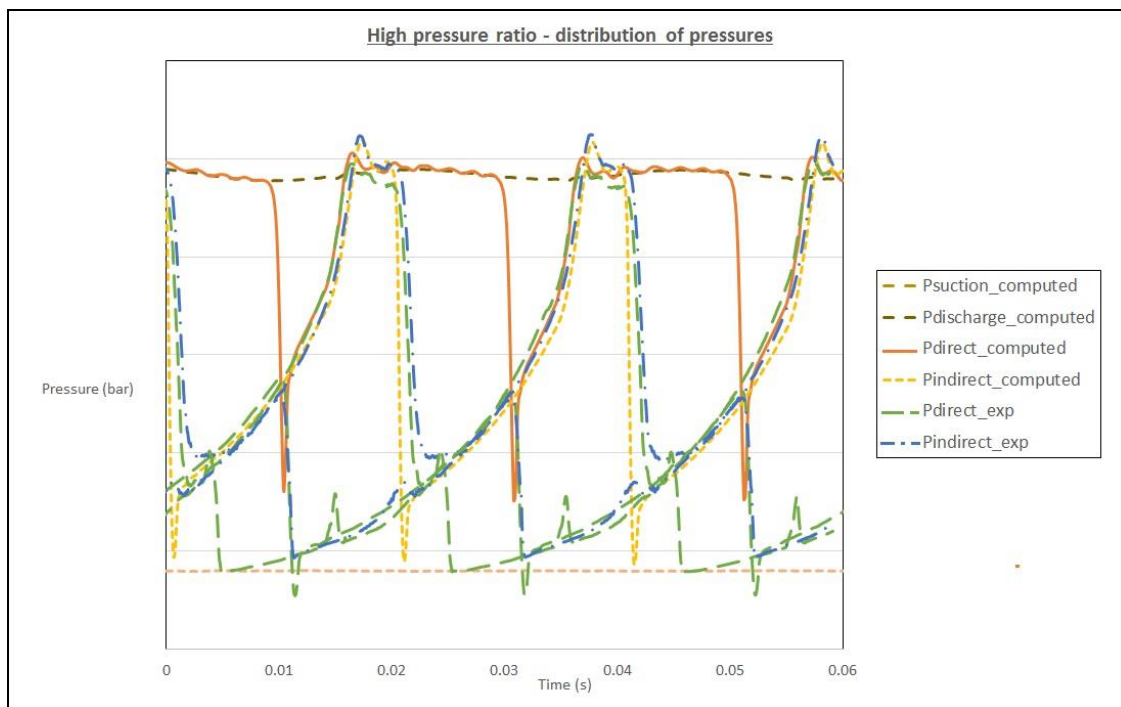
The major interest of this study is the comparison of the predicted pocket pressures with experimental data (data which was acquired in previous experimental tests using thinly instrumented compressors).

Figure 4 shows the distribution of pressures along the compression paths, direct and indirect pockets and from suction to discharge, for the ARI point. Comparing the slopes of the experimental and the computed curves, we can once again check the validity of the modelling assumptions: too high rates of leakages would have led to significantly diverging curves. There is good agreement between the predicted and measured data. The slight overcompression currently seen at the discharge point is also visible in the simulation results.



**Figure 4** : pressure distributions during the compression process at ARI conditions

Figure 5 presents the same comparison but at the high pressure ratio operating point. The agreement between simulated and computed data remains correct, including the inflexion of pressure at the beginning of the discharge process due to the back flow from the upper shell to the pockets. The differences between the pressure distributions in the direct and indirect paths are also well represented, with the flow area being much higher at that time between the direct pockets and the discharge port.



**Figure 5** : pressure distributions at high pressure ratio

Figure 6 presents the pressure distribution at the low pressure ratio. These operating points result in a huge overpressure in the pockets with respect to the upper shell. At this ratio, the results appear slightly less precise, especially at the end of the compression process. The CFD results show an increase in the difference between the pressures in the direct and indirect paths when compared to experimental data and the maximum pressure is over predicted. This illustrates one difficulty of simulating such operating points, where volumes at significantly different pressures get connected, resulting in high velocity flows. Capturing them well would require lower time steps and refined meshes in these zones.

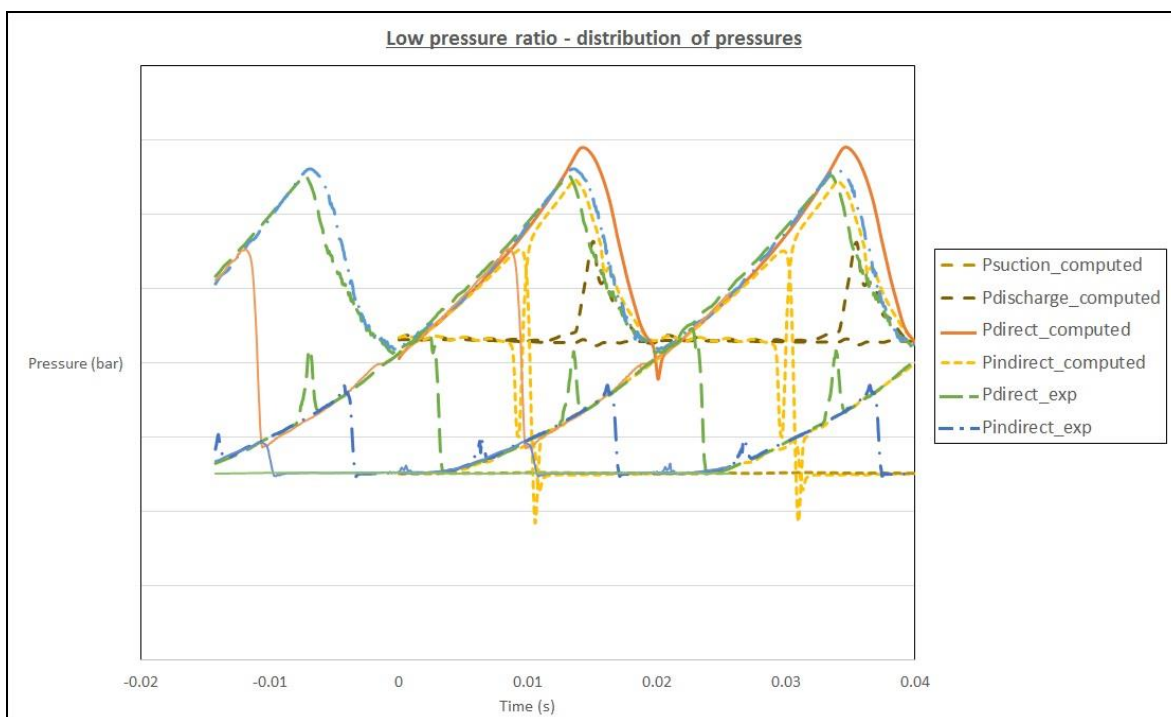


Figure 6 : pressure distributions at low pressure ratio

### 3.3 Analysis of the flow field

#### 3.3.1 Suction

Figure 7 presents the velocity magnitude on a horizontal plane at scroll mid-height. High velocity gradients near the inlet zones can be seen. Here, the widening of the suction area results in an acceleration of the fluid which, coupled to the necessity to pass around the edge of the wraps, leads to a separated flow. Lowering the intensity of this phenomenon would bring higher volumetric efficiencies.

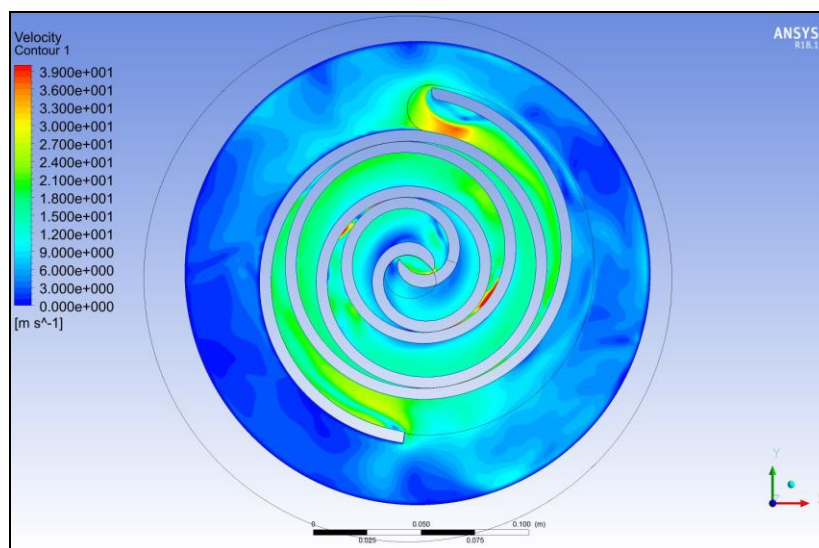
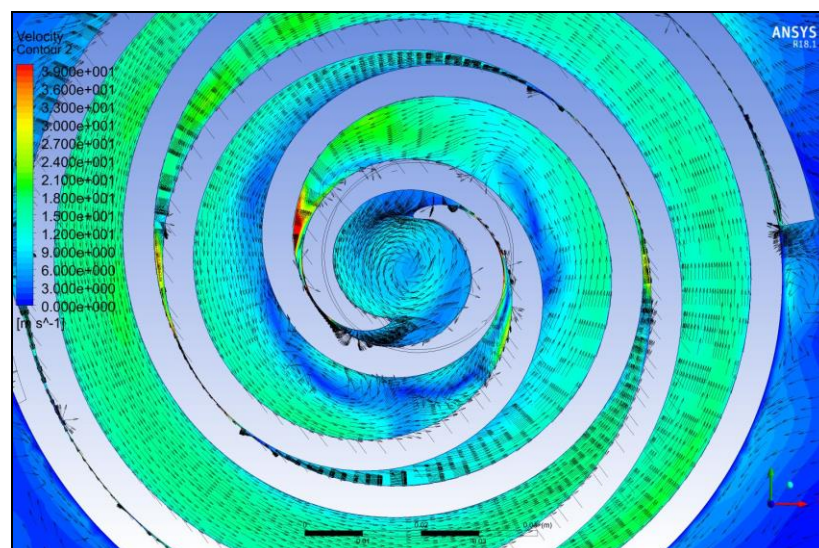


Figure 7 : velocity contours

Figure 8 shows an interesting and quite surprising fluid dynamic phenomenon. In the intermediate pockets, zones of low velocity and high vorticity appear even though the discharge point has not yet been reached. It can be observed that the flow separates on the inner part of the pockets, in the region of maximal curvature. Though the recirculation areas are not close to the sealing points, a deeper analysis would perhaps show that the vortices are driven by the leakage flows going from the high pressure pockets.

Improving the reliability of the physical representation of the flow would require the use of non-isotropic turbulence model, e.g. a Reynolds Stress turbulence model, which is much more time consuming.



**Figure 8** : superimposition of velocity vectors and velocity contours

### 3.3.2 Discharge at high pressure ratio

Considering the high pressure ratio condition, when the discharge port opens, the pocket pressures are far lower than that in the upper shell. Hence, compression is achieved not only by the volume reduction in the pockets but also by the fluid transfer from a high pressure volume to a low pressure one, explaining the inflexion of the pressure curves seen in figure 5.

Figure 9 shows the velocity contours in the scroll every 4 degrees. As the pockets open onto the discharge port (frame 1 to frame 12) the high speed jet filling the pockets (frames 2 to 5) can be clearly seen, followed by lower intensity jets blowing off the pockets (frames 11 and 12).

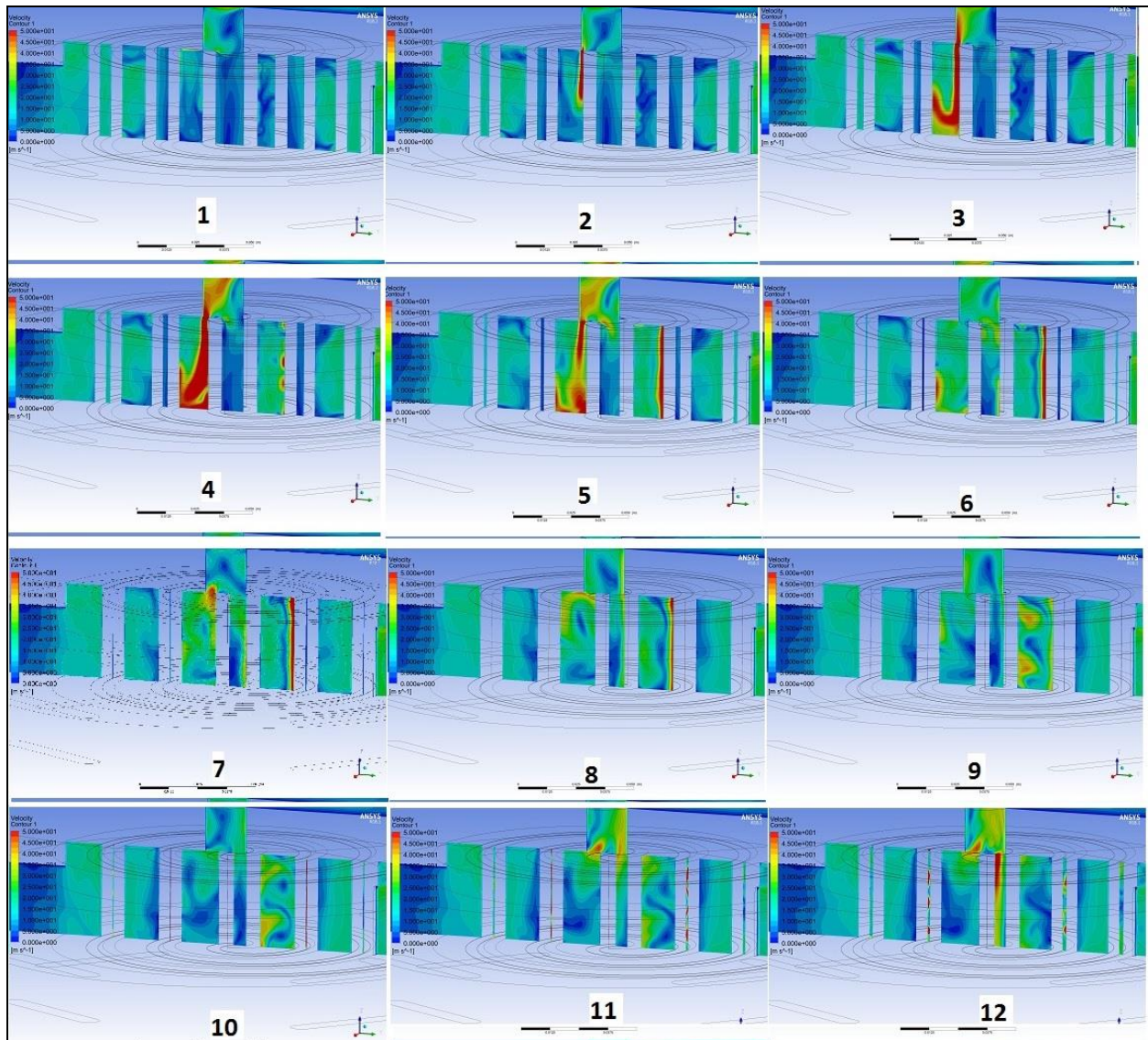


**Figure 9** : Velocity contours in an meridian plane at high pressure ratio

